Journal of Chromatography A, 1429 (2016) 304–310

Contents lists available at ScienceDirect

Journal of Chromatography A

journal homepage: www.elsevier.com/locate/chroma

Characterization of ultrahigh-molecular weight cationic polyacrylamide using frit-inlet asymmetrical flow field-flow fractionation and multi-angle light scattering

Sohee Woo [a], Ju Yong Lee [a], Woonjin Choi [b], Myeong Hee Moon [a,*]

[a] Department of Chemistry, Yonsei University, Seoul 120-749, South Korea
[b] Kolon Life Science Inc., 13 Kolon-ro, Gwacheon-si, Gyeonggi-do 427-709, South Korea

ARTICLE INFO

Article history:
Received 21 October 2015
Received in revised form 7 December 2015
Accepted 8 December 2015
Available online 11 December 2015

Keywords:
Cationic polyacrylamide
C-PAM
Branched
Molecular weight determination
Field-flow fractionation
Multi-angle light scattering

ABSTRACT

In this study, frit inlet asymmetrical flow field-flow fractionation (FlFFF) with multi-angle light scattering (MALS) and differential refractive index (DRI) detection is utilized for size separation, determination of molecular weight (MW), and conformation of ultrahigh-MW (10^7–10^9 g/mol) cationic polyacrylamides (C-PAMs), a class of water-soluble copolymers based on acrylamide and vinyl-type comonomers with quaternary ammonium cations that are widely used in wastewater treatment and in paper industries. Linear and branched C-PAM copolymers prepared in two different polymerization methods (solution and emulsion) from varying amounts of crosslinking agent and initiator were size fractionated by FlFFF with field-programming. It was found experimentally that the linear copolymers from both polymerization methods were less than 10^8 g/mol in MW with compact, nearly spherical structures, while the branched C-PAM copolymers from the emulsion polymerization showed a significant increase in average MW up to ~10^9 g/mol, which was about 20-fold greater than those from the solution method, and the branched copolymers had more compact or shrunken conformations. While both linear and branched copolymers less than 10^8 g/mol MW were well resolved in an increasing order of MW (normal mode), it was noted that branched copolymers prepared through emulsion polymerization exhibited significantly larger MWs of 10^8–10^9 g/mol and eluted in the steric/hyperlayer mode, in which the elution order is reversed in an extreme run condition (strong initial field strength followed by a fast field decay during programming).

1. Introduction

Cationic polyacrylamides (C-PAMs) are a class of water-soluble acrylamide-based polymers copolymerized with a vinyl-type comonomer having quaternary ammonium cations [1–3]. Acrylamide-based homopolymers (PAMs) are water soluble and are important in a number of industrial applications such as flocculants in paper manufacturing [4,5], enrichment/recovery of minerals from mining [6], wastewater treatment [7], and as rheology control agents [8]. However, due to the nonionic nature of PAMs, the incorporation of a charged group into an acrylamide chain provides a polyelectrolyte-like property, which results in a markedly improved performance in flocculation compared to that of nonionic PAMs. Specifically, C-PAM copolymers have been widely used as flocculants in paper manufacturing [2,9] and waste water treatment [7,10].

C-PAM copolymers are synthesized with acrylamide (AM) and cationic comonomers of quaternary nitrogen-containing structures such as acryloxyethyltrimethyl ammonium chloride (DAC) [10,11], methacryloxyethyl ammonium chloride (DMC) [12], acryloxyethyl dimethylbenzyl ammonium chloride (AODBAC) [13,14], etc. [1]. Since a branched polymer has a relatively lower viscosity than a linear polymer of the same molecular weight (MW), along with improved solubility in water, branched copolymers exhibit better performance [15,16]. The efficiencies of C-PAM copolymers as flocculants are known to depend on a number of parameters, including MW, molecular conformation, and degree of charge density [2,14]. Specifically, the determination of accurate MW and molecular weight distribution (MWD) of C-PAM is important in controlling the material properties in accordance with the

* Corresponding author: Fax: +82 2 364 7050.
E-mail address: mhmoon@yonsei.ac.kr (M.H. Moon).

http://dx.doi.org/10.1016/j.chroma.2015.12.027
0021-9673/

intended applications. Size characterization of typical branched C-PAM molecules (<10^7 g/mol) has often been carried out using intrinsic viscosity measurement [11], size exclusion chromatography (SEC) based on calibration using PAM standards [13,14], or on multi-angle light scattering (MALS) analysis [17]. However, for ultrahigh-MW C-PAM molecules (>10^7), the determination of average MW has relied on intrinsic viscosity measurements [2] or on batch analysis using MALS [3] due to the lack of relevant SEC columns having packing materials of sufficient pore sizes to accommodate ultrahigh-MW molecules. In the case of the viscosity measurements, while branched polymers exhibit viscosity values lower than linear polymers of the same MW, it is complicated to determine accurate MWs and MWDs of ultrahigh-MW C-PAM materials. Even with SEC, ultrahigh-MW C-PAM molecules often shrink, resulting in difficulties in determining accurate MWs due to the addition of a considerable amount of salts in the mobile phase for successful elution through the SEC column.

Flow field-flow fractionation (FlFFF) is an elution-based method that is capable of separating macromolecules according to hydrodynamic size and has been widely utilized for characterization of polymers (both aqueous and organic) and proteins as well as nano- and micro-sized particles including those having biological importance such as exosomes, cells, and subcellular organelles [18–22]. Separation in FlFFF is carried out in an unobstructed rectangular channel space without a stationary phase by utilizing two flow streams (a migration flow to drive sample components down the channel and a cross flow moving across the channel to retard the migration of sample species) [23]; therefore, it is rather well suited to handle ultrahigh-MW species without danger of sample loss. Since the separation of components in the typical normal mode of FlFFF is achieved by an increasing order of diffusion coefficients of the sample materials and thus their hydrodynamic diameters [18], the online use of FlFFF with MALS (FlFFF-MALS) offers an outstanding feature for separation and MW characterization of various water-soluble polymers such as polysaccharides [24], polyacrylamides [25], amylopectin [26,27], and hyaluronic acid [28–32].

In this study, ultrahigh MW (10^7–10^9 Da) C-PAM copolymers synthesized from AM monomers with a cationic comonomer, DAC, were examined using FlFFF-MALS. The FlFFF system employed in this work was a frit inlet asymmetrical FlFFF (FIAF4) channel [33], which is a modified form of asymmetrical FlFFF utilizing the hydrodynamic relaxation of sample components without the focusing/relaxation method that has been commonly applied for conventional asymmetrical FlFFF. With hydrodynamic relaxation, sample components injected into the channel are expected to achieve equilibrium between the two counter-directed forces (the external field force generated by the crossflow and the diffusion of components against the channel wall) while they continuously migrate through the channel. The C-PAM copolymers examined in this study were synthesized using two different polymerization methods, solution polymerization and emulsion polymerization, by varying the amount of an initiator with or without addition of a cross-linking agent. Thus, the effects of polymerization method and branching on MW, MWD, and molecular confirmation of C-PAM could be examined using FIAF4 with MALS. While most of the C-PAM species examined in this work were analyzed in normal mode of FlFFF separation, we observed that a few extremely high-MW branched C-PAM species were separated by steric/hyperlayer elution mode. Steric/hyperlayer elution is typical for the separation of micronsized particles since diffusion of larger particles becomes negligible and particles are lifted from the channel wall by hydrodynamic lift forces, therefore larger species elute more rapidly than smaller ones [34]. While the steric/hyperlayer elution is common with miconsized particles, it has not been found for polymeric species in FlFFF to the best of our knowledge.

2. Experimental

2.1. Materials and reagents

The C-PAM copolymer samples examined in this study were poly(acrylamide-co-N,N,N-trimethyl aminoethyl chloride acrylate) synthesized from AM monomers copolymerized with DAC. Eight C-PAM copolymer samples were obtained in powdered form from Kolon Life Science Inc. (Gwacheon, Korea) and were synthesized using two different polymerization methods (solution polymerization and emulsion polymerization) by varying the amounts of cross-linking agent, initiator, and chain transfer agent in order to form linear and branched polymers of different MWs, as listed in Table 1. The identification of each sample shown in Table 1 is designated with L for linear polymers, B for branched polymers, S for solution polymerization, and E for emulsion polymerization. To prepare aqueous solutions, copolymer samples were dissolved in deionized water (>18 MΩ) at a concentration of 0.5 mg/mL by stirring at 300 rpm for 2 h using a glass-blade impeller installed in a WiseStir® HS-30E model stirrer from Daihan Scientific Co. (Wonju, Korea) and reducing the stirring rate to 150 rpm for 22 h. Next, $NaNO_3$ from Sigma–Aldrich Co. (St. Louis, MO, USA) was added to the dissolved C-PAM samples to produce a total 0.1 M $NaNO_3$ solution (300 rpm for 30 min) for FIAF4-MALS analysis.

2.2. FIAF4-MALS

The FIAF4 channel utilized in this study was modified from an Eclipse® channel model LC (long channel) from Wyatt Technology Europe GmbH (Dernbach, Germany) by replacing the inlay (a plastic block used as a depletion wall) with a frit-inlet type of inlay equipped with a ceramic inlet frit (35 mm × 18 mm × 7 mm) at the inlet end of the polycarbonate inlay, as described in a previous study [32]. Through the inlet frit, a tubing port was created by drilling a hole to insert a Teflon tube (0.03 inch i.d. and 1/16 inch o.d.) for the channel inlet so that the sample materials could be delivered to the FIAF4 channel. The channel spacer was a 195-μm-thick Mylar sheet cut into a trapezoidal channel design having an initial breadth of 1.6 cm, which decreased to 0.4 cm at the outlet end. The length of the channel was 26.5 cm, with triangular sections at both ends. The actual length of the inlet frit exposed to the channel space was 3.5 cm. At the accumulation wall, a regenerated cellulose membrane from Microdyn-Nadir GmbH (Wiesbaden, Germany) with a pore size of 10 kDa was placed above the stainless steel frit. A model 7725i loop injector from Rheodyne (Cotati, CA, USA) was installed between the channel inlet and a model SP930HPLC pump from Young-Lin Co. (Seoul, Korea) for sample loading. Frit inlet flow was delivered from a model 1260 Infinity HPLC pump from Agilent Technologies (Palo Alto, CA, USA), and the flow rates were controlled (frit flow, cross flow, and outflow) with the Eclipse system from Wyatt Technology Europe GmbH. The carrier solution of FIAF4 (for both sample injection flow and frit flow) was prepared with deionized water (>18 MΩ) containing 0.1 M $NaNO_3$ and 0.02% NaN_3 from Sigma-Aldrich as bactericide, and the prepared solution was filtered through a Durapore® Membrane filter (0.1 μm pore, polyvinylidene fluoride) from Merck Millipore (Darmstadt, Germany) prior to use. To remove any particulate species contained in the carrier solution, a PEEK inline filter unit with a VVLP membrane with 0.1-μm pores from Wyatt Technology Europe GmbH was placed right after the outlet of each pump.

FIAF4 operation was achieved through hydrodynamic relaxation, in which samples were injected through the inlet of the channel while a high-speed frit flow (more than 20 times faster than the sample stream) was introduced through the inlet frit so that the sample components could be pushed toward the accumulation wall of the channel to achieve equilibrium during continuous

Table 1
Types of C-PAM copolymer samples used for FIAF4-MALS analysis.

ID	Structure	Polymerization	Initiator	Chain transfer agent	Cross-linking agent	dn/dc	Decay pattern*
LS1	Linear	Solution	High	High		0.1647	1
LS2		Solution	Low	Low		0.1579	1
LE1		Emulsion		High		0.1093	2
LE2		Emulsion		Low		0.1614	3
BS1	Branched	Solution			High	0.1394	2
BS2		Solution			Low	0.2631	2
BE1		Emulsion			High	0.1073	2
BE2		Emulsion			Low	0.2115	2

* Linear decay patterns of crossflow rates in mL/min (elapsed time in min).
1: 2.0 (4) → 0.5 (5) → 0.1 (2) → 0.02 (5)
2: 2.5 (4) → 0.5 (2) → 0.1 (2) → 0.02 (3)
3: 2.5 (4) → 0.5 (5) → 0.1 (2) → 0.02 (5)
4: 2.5 (4) → 0.5 (7) → 0.1 (5) → 0.02 (9)

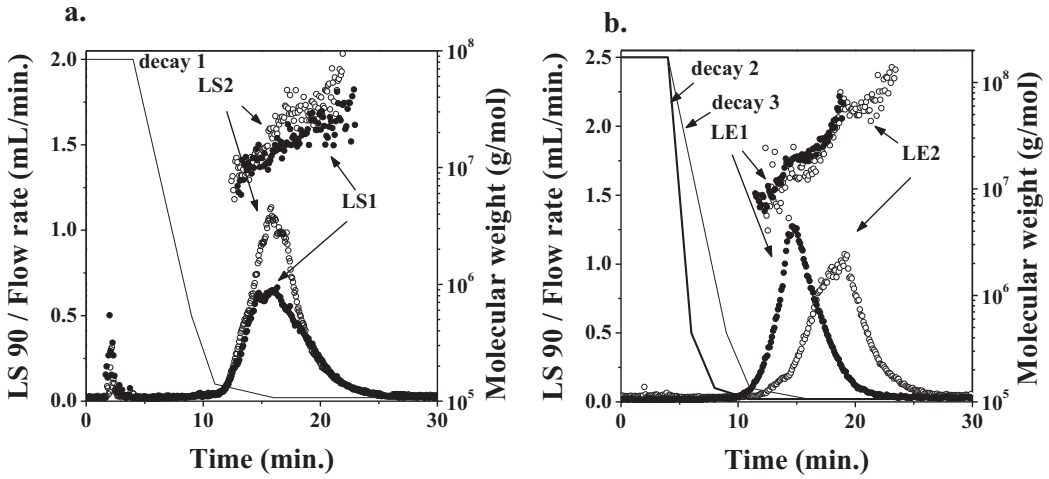

Fig. 1. (a) Superimposed fractograms (based on light scattering at 90°) of linear C-PAM copolymers prepared through solution polymerization (LS1 and LS2), and calculated MW data points obtained using FlFFF-MALS-DRI. Decay pattern 1 represents the linear programming of the crossflow rate during elution. (b) Fractograms of copolymers from emulsion polymerization (LE1 and LE2) obtained using decay patterns 2 and 3, respectively.

migration. Sample injections were made at 0.1 mL/min throughout the runs, which was the same as the outflow rate to the detector. The crossflow rate was adjusted to be the same as the frit flow rate, which decreased as multistep linear decay patterns were used during runs by varying the decay periods depending on the MW distribution of the C-PAM copolymer samples. Three different decay patterns of frit flow (same as crossflow) rate were utilized, as marked in the run conditions listed in Table 1. Run condition 1 began at 2.0 mL/min of crossflow rate for 4 min and then linearly decreased to 0.5 mL/min over 5 min, to 0.1 mL/min over 2 min, to 0.02 mL/min over 5 min, and was then maintained [expressed as 2.0 (4) → 0.5 (5) → 0.1 (2) → 0.02 (5)]. Run conditions 2 and 3 both began with a higher crossflow rate of 2.5 mL/min but had different decay patterns, as listed in Table 1. The C-PAM materials eluted from the FIAF4 channel were detected serially with a DAWN-DSP MALS detector at a wavelength of 632.8 nm and a differential refractive index (DRI) of 658 nm with an Optilab T-rEX detector (both from Wyatt Technology, Santa Barbara, CA, USA). Recordings of detector signals were made using ASTRA software from Wyatt, and baseline drifts in DRI detection caused by flow programming were corrected by subtracting a blank run obtained before or after each sample run in ASTRA. Calculations of C-PAM MW were based on the use of MALS signals at detector angles of 38.0°, 44.0°, 50.0°, 57.0°, 64.0°, 72.0°, and 81.0° with measured dn/dc values. The measurements of the dn/dc values listed in Table 1 were made for each sample by sequentially injecting diluted sample solutions of eight different concentrations into the Optilab T-rEX DRI detector and calculating the values using ASTRA.

3. Results and discussion

Eight C-PAM copolymer samples prepared using both solution and emulsion polymerization methods with or without incorporating branching structures were analyzed using FIFFF-MALS combined with DRI (FlFFF-MALS-DRI) and different field-decay patterns, in which the crossflow rates were programmed to decrease during elution. Fig. 1a shows the superimposed fractograms (LS90: light scattering signals at 90°) of two linear C-PAM copolymers (LS1 and LS2) prepared through solution polymerization using the linear decay pattern 1 (see Table 1). The notifications for the eight samples are classified as follows: L and B stand for linear and branched polymers, respectively, S stands for solution polymerization, and E for emulsion polymerization, as listed in Table 1. The elution profiles of both LS samples appear to be similar, and the calculated MW values at each time slice from MALS, which are plotted above the two fractograms with the same symbol for each sample, appear to gradually increase as retention time increases, indicating that the normal mode of FlFFF separation was achieved for these two samples. However, the MW values of LS2 after 10^7 g/mol increase at a slightly steeper rate than those of LS1 with the increase in

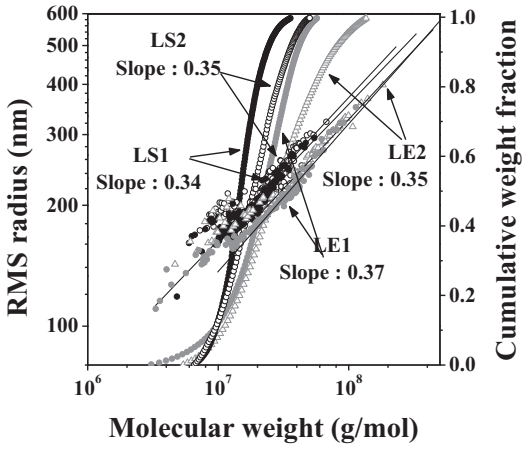

Fig. 2. Superimposed cumulative weight distribution curves of the four linear copolymers along with the plots of RMS radius vs. MW in logarithmic scale. Slope values were obtained from the linear regression of data points.

retention time, implying that the molecular conformations of these two samples differ to some degree. For the two other linear copolymer samples (LE1 and LE2) prepared through emulsion polymerization, a similar pattern of increasing MW values is shown in Fig. 1b. The LE samples were run with field-decay patterns 2 and 3 for LE1 and LE2, respectively, since the hydrodynamic relaxation of these samples was not successful until the initial crossflow rate was increased to 2.5 mL/min due to the MW increase (up to 10^8). However, both samples were smoothly resolved using the different decay patterns.

Fig. 2 presents the cumulative weight distribution curves of LS1, LS2, LE1, and LE2 along with plots of the root mean square (RMS) radius versus MW. Based on the MWD curves and average MW (or Mw) values of the linear chain C-PAM copolymers in Table 2, LS1 and LS2 exhibited similar distributions, except that LS2, formed with a lesser amount of initiator, yielded an increase in Mw from 1.45×10^7 to 1.86×10^7 g/mol. We noted that emulsion polymerization resulted in a much higher Mw (3.02×10^7 g/mol for LE2) for linear C-PAM copolymers with a broader MWD than did solution polymerization. However, the slope values, which represent the molecular conformation in solution, were within 0.34–0.37 (standard deviation less than 0.01, $n = 3$) as listed in Table 2, supporting that these four linear chain copolymers were relatively compact regardless of polymerization method. Relatively compact structures of the linear polymers can be from either by intramolecular interaction of ultrahigh MW polymers or a solvent condition between the non-perturbed theta state and the critical solution conditions.

The FlFFF-MALS-DRI results for the two branched copolymers (BS1 and BS2) in Fig. 3a shows a distinct difference in peak distribution. Both were obtained with field-decay pattern 2. A higher initial crossflow rate (adjusted to be the same as the frit flow rate) was needed for these branched copolymer samples in order to achieve successful hydrodynamic relaxation of the ultrahigh-MW species since some species were incompletely relaxed with field-decay pattern 1, resulting in a shoulder peak at the beginning of the elution (7–10 min, not shown here). With pattern 2, the shoulder peaks before 10 min were nearly minimized, as shown in Figure 3a. This supports the hypothesis that the diffusional activity of branched molecules due to their compact or shrunken structures becomes faster than that of the linear copolymer samples, although the MW ranges of the BS molecules were similar to those of the LS samples. Compared to the fractogram and calculated MW points of LE1 superimposed in Figure 3a, molecules in BS1 eluted earlier than those of same MW in LE1, supporting that the effect of branching changed the diffusion properties. BS2, with a relatively lesser amount of crosslinking agent than BS1, rapidly increased in peak concentration at the beginning of elution. By comparing the calculated MW points of the two branched samples above the fractograms, we noted that the BS2 copolymers eluted more slowly than BS1 molecules of an identical MW after 10 min, which corresponds to MW > 10^7 g/mol, as the retention time increased. This might be due to the differences in copolymer structures. Due to the use of crosslinking agent, branching together with the effect of imperfect solution condition resulted in the formation of more compact structures than those of the linear polymers. A branched C-PAM copolymer sample with an increased amount of crosslinking agent might accelerate the degree of branching during polymerization, which could make BS1 more compact than BS2. Since the FlFFF retention of macromolecules depends on the hydrodynamic size of the molecules, the copolymers with expanded structures have effectively large hydrodynamic radii and are thus retained longer than the spherical ones of an equivalent molecular weight. Therefore, BS1 can be expected to elute earlier than BS2 of an equivalent MW. This will be explained further with RMS plots later.

Branched copolymer samples prepared with emulsion polymerization method (BE1 and BE2 differing by amounts of crosslinking agent) exhibited a steric/hyperlayer separation in which large molecules elute earlier than smaller ones as shown in Fig. 3b due to the roles of hydrodynamic lift forces. These were obtained with the same field-decay pattern 2 used for Fig. 3a. Since molecular weights of the two BE samples range as 10^8–10^9 g/mol in Fig. 3b, these copolymers appeared to elute in an opposite trend to those observed in Fig. 3a. Since steric/hyperlayer elution of polymeric materials has not been reported, elution patterns of BE samples were examined by varying decay patterns in Fig. 4. Separation of BE1 with the decay pattern 3 shows an apparently uniform Gaussian distribution in the fractogram (triangles). However, calculated MW points show two different elution patterns, in which the MW decreased from the beginning of the elution until 15 min (from 10^9 to 10^8 g/mol), and then this pattern was reversed after 15 min. When the crossflow was adjusted to decay more slowly (decay pattern 4), the retention of molecules was elongated to longer time periods, but the calculated MW points (stars)

Table 2
Calculated average values ($n = 3$) of Mw, Mn, polydispersity, Rz, Rn, and slope of C-PAM copolymers obtained by FlFFF-MALS-DRI.

	Mw (g/mol)	Mn (g/mol)	Polydispersity	Rz (nm)	Rn (nm)	Slope
LS1	$(1.45 \pm 0.10) \times 10^7$	$(1.12 \pm 0.30) \times 10^7$	1.28 ± 0.30	192.2 ± 4.6	182.2 ± 3.6	0.34 ± 0.00
LS2	$(1.86 \pm 0.09) \times 10^7$	$(1.54 \pm 0.08) \times 10^7$	1.21 ± 0.00	213.7 ± 1.3	199.7 ± 0.6	0.35 ± 0.01
LE1	$(2.47 \pm 0.01) \times 10^7$	$(2.03 \pm 0.05) \times 10^7$	1.22 ± 0.03	189.4 ± 3.8	173.3 ± 2.3	0.37 ± 0.01
LE2	$(3.02 \pm 0.08) \times 10^7$	$(1.93 \pm 0.03) \times 10^7$	1.57 ± 0.18	254.4 ± 2.1	212.1 ± 5.1	0.35 ± 0.01
BS1	$(2.06 \pm 0.07) \times 10^7$	$(1.61 \pm 0.10) \times 10^7$	1.28 ± 0.03	222.9 ± 3.8	206.4 ± 0.6	0.26 ± 0.00
BS2	$(1.67 \pm 0.01) \times 10^7$	$(1.40 \pm 0.25) \times 10^7$	1.22 ± 0.20	217.7 ± 8.0	203.6 ± 3.5	0.28 ± 0.00
BE1	$(4.60 \pm 0.09) \times 10^8$	$(3.78 \pm 0.45) \times 10^8$	1.22 ± 0.15	579.4 ± 0.1	464.1 ± 5.4	0.30 ± 0.01
BE2	$(3.56 \pm 0.07) \times 10^8$	$(2.90 \pm 0.02) \times 10^8$	1.23 ± 0.04	441.5 ± 7.4	366.0 ± 2.9	0.35 ± 0.01

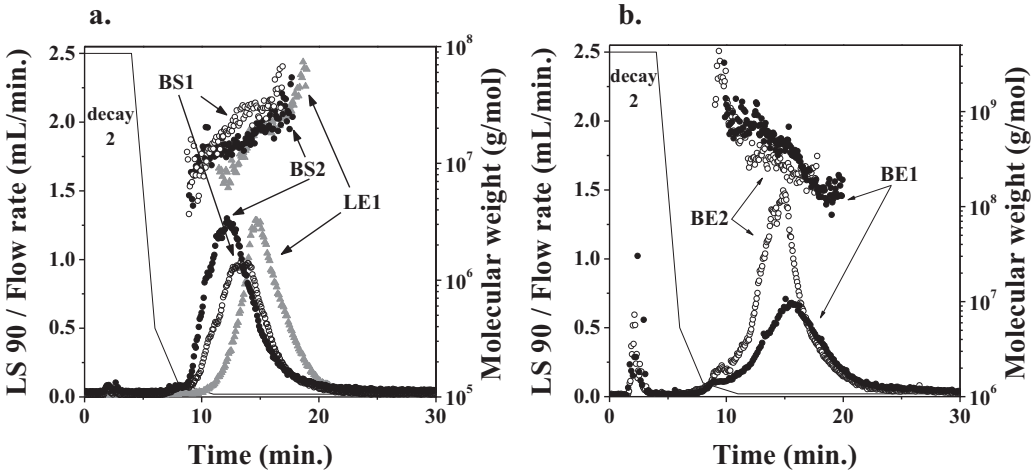

Fig. 3. Superimposed fractograms of the two branched C-PAM copolymers from (a) solution polymerization (BS1 and BS2) in the normal mode of FlFFF and (b) emulsion polymerization (BE1 and BE2) along with calculated MW data points showing the steric/hyperlayer elution mode of FlFFF.

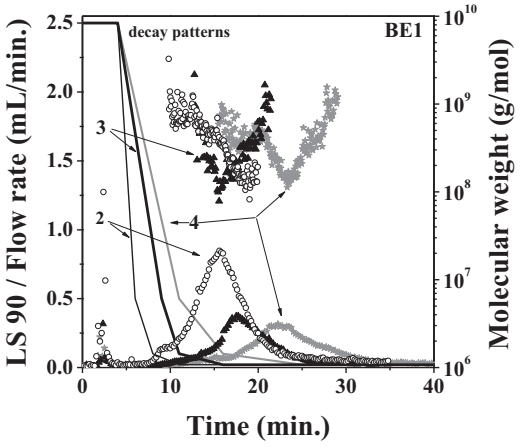

Fig. 4. Effect of decay pattern on the elution profiles of BE1 according to FlFFF-MALS-DRI, showing that a faster decay in crossflow rate (decay pattern 2) is conducive to eluting ultrahigh-MW species in steric/hyperlayer mode without splitting in elution mode with increased peak recovery.

exhibited a similar interruption. Since field strength decays during the passage of time and sample components are relaxed hydrodynamically, it is rather complicated to observe a distinct, but sharp peak showing a steric transition. It is thought that the ultrahigh-MW species examined in this study migrate in a mixed mode of operations (normal and steric/hyperlayer), as shown in the separations with decay patterns 3 and 4, when hydrodynamic relaxation is not quickly accomplished for the entire MW range of molecules. For instance, during the hydrodynamic relaxation, ultrahigh-MW polymers require a higher frit flow rate (equivalent to the crossflow rate) for a complete hydrodynamic relaxation; however, at the same time, larger species experience stronger hydrodynamic lift forces than smaller ones. Therefore, it is possible for very large branched molecules (MW > 10^8) to achieve steric/hyperlayer elution. When the field strength starts to decay, migrating sample components achieve secondary relaxation in which sample components achieve new equilibrium heights depending on the balance of two counter-directing forces (field force versus lift forces plus diffusion). As the field strength decreases to a level where hydrodynamic lift forces are not dominant, the sample components rely on the diffusional activity, gaining force balance to follow the normal mode of migration. A possibility cannot be excluded that some species, which are temporarily captured at the membrane surface due to the high initial field strength, are released from the surface after the field strength is reduced and then migrate in normal mode. To avoid these abnormal observations in the separation of ultrahigh-MW species, an experimental trial was designed such that steric/hyperlayer elution should be accomplished in a short time period. When decay pattern 2 was employed (a faster decay period), the peak intensity was significantly increased, and the calculated MW values (open circles) during the elution periods of 8–20 min gradually decreased without significant turnover, supporting that the ultrahigh-MW species successfully eluted in steric/hyperlayer mode with a more rapid field decay (crossflow rate). In addition, it is noteworthy that branched copolymers larger than 10^8 g/mol can be separated in steric/hyperlayer elution mode, as seen by comparing the separations in Figs. 3a and b. The calculated average RMS radius (R_w) values were 520 nm and 400 nm for BE1 and BE2, respectively, which are equivalent to 1.4–0.8 μm in average diameter. It is known that the steric transition of spherical particles in asymmetrical FlFFF can be observed at or around 0.5 μm of Stokes diameter [35], indicating that the branched C-PAM copolymers in Fig. 3b are resolved under steric/hyperlayer mode.

Molecular weight distributions and RMS plots of the branched C-PAM copolymers depending on polymerization method are compared in Fig. 5. When the RMS plot of BE1 is compared with that of LE1 in Fig. 5a, both formed using emulsion polymerization, there is a distinct difference in MW range between the linear (Mw 2.5×10^7–3.0×10^7 g/mol) and branched polymers (Mw 3.6×10^8–4.6×10^8 g/mol), with a substantial decrease in the slope value (from 0.37 ± 0.01 to 0.30 ± 0.01) of the branched copolymers. When the branched copolymers synthesized with different polymerization methods are compared with each other in Fig. 5b, it is evident that the branched C-PAM copolymers from emulsion polymerization yielded an increase (~20-fold) in Mw, in contrast to those from solution polymerization. However, we noted that the Mw values of the branched copolymers from both polymerization methods increased with an increase in the crosslinking agent amount. While the slope values of the RMS plots for the BS samples are 0.26 ± 0.00 and 0.28 ± 0.00, those of the BE samples are 0.30 ± 0.01 and 0.35 ± 0.01, indicating that the solution-polymerized BS samples were more compact in their branched copolymer structures than were the BE samples. Moreover, the RMS plots of the two BS samples in Fig. 5b show that both slope values were smaller than those of the linear copolymers (~0.35 for LS samples) in Fig. 2, indicating the marked reduction in

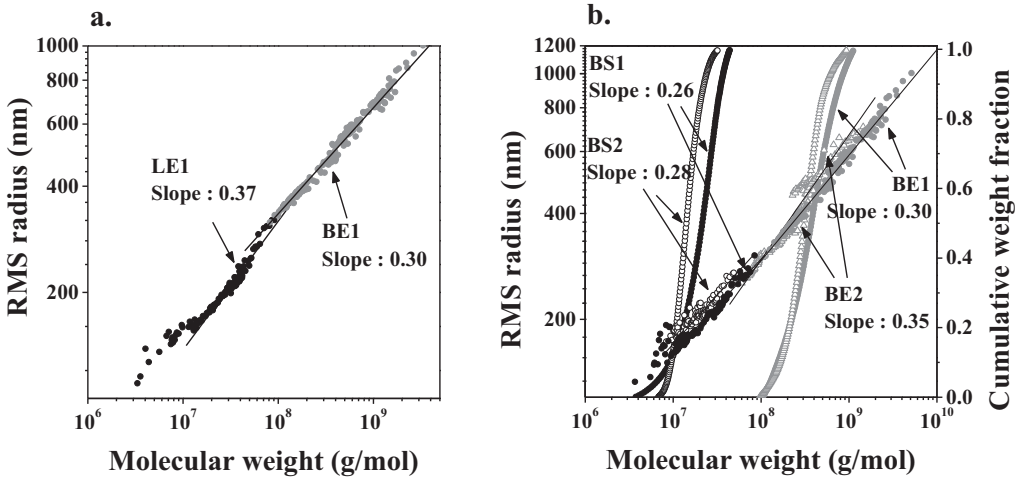

Fig. 5. (a) Comparison of RMS radius plots (vs. MW) of LE1 and BE1, and (b) superimposed cumulative weight distribution curves of the four branched C-PAM copolymers along with RMS plots.

the structures due to crosslinking. We noted that the RMS radius values of BS2 (open circles) are larger in the region of MW > 10^7 g/mol than those of BS1 (filled circles), as shown in the lower left of Fig. 5b, which implies that the molecular structures of BS2 were slightly more extended than those of BS1. This corresponds to the finding in Fig. 3a that BS1 molecules (>10^7 g/mol) of an equivalent MW eluted slightly earlier than BS2 molecules. However, the Mw values of both BS samples were not significantly changed from those of the LS samples listed in Table 2. This might be because the molecular structures of branched C-PAM copolymers synthesized using the solution polymerization method can be formed in a more compact way while maintaining a similar Mw. However, we found that emulsion polymerization induces a significant increase in the Mw of C-PAM copolymers due to the branching effect, while it causes a moderate increase in the Mw of linear copolymers.

4. Conclusion

This study shows that FlFFF-MALS-DRI experiments with field-programmed separation can be powerfully utilized for size separation and MW characterization of ultrahigh-MW (10^7–10^9 g/mol) linear and branched C-PAM copolymers, which are difficult to analyze with typical viscometric measurements or SEC. Linear C-PAM copolymers prepared from solution and emulsion polymerization methods were found to be in the MW range of 10^7–10^8 g/mol, with a broader size distribution produced when using the emulsion method. However, the molecular conformations from RMS radius versus MW plots show a similar compact geometry for the two polymerization methods. Branched C-PAM copolymers formed through the solution polymerization method showed a moderate increase (~two-fold) in Mw compared to those of linear copolymers, together with more compact molecular geometries due to the incorporation of crosslinking. In contrast, the Mw values of the branched materials synthesized through the emulsion method were significantly increased to ~4×10^8 g/mol, nearly 20 times larger than those formed with the solution method. In addition, branched copolymers larger than 10^8 g/mol could be separated in steric/hyperlayer elution mode, which is unusual in the FlFFF separation of water-soluble macromolecules, while those smaller than 10^8 g/mol were separated in the normal mode of elution. We found experimentally that the steric inversion of ultrahigh-MW copolymers occurred at MWs of ~10^8 g/mol when field programming was applied with hydrodynamic relaxation in the frit inlet asymmetrical FlFFF channel. In addition, experiments showed that a strong initial field strength was required for efficient hydrodynamic relaxation of ultrahigh-MW species at the beginning of separation with a fast field decay so that such large species can elute expeditiously in steric/hyperlayer mode. Otherwise, some species that can be undesirably trapped at the channel membrane during the high initial field might release from the wall and migrate along the normal mode of elution pattern when the field slowly decays, which is caused by a decrease in hydrodynamic lift forces.

Acknowledgements

This study was supported by a grant (2015R1A2A1A01004677) from the National Research Foundation of Korea.

References

[1] W. Jaeger, J. Bohrisch, A. Laschewsky, Synthetic polymers with quaternary nitrogen atoms-synthesis and structure of the most used type of cationic polyelectrolytes, Progress in Polym Sci. 35 (2010) 511–577.
[2] E. Antunes, F.A.P. Garcia, P. Ferreira, A. Blanco, C. Negro, M.G. Rasteiro, Use of new branched cationic polyacrylamides to improve retention and drainage in papermaking, Ind. Eng. Chem. Res. 47 (2008) 9370–9375.
[3] K.A. Klimchuk, M.B. Hocking, S. Lowen, Water-soluble acrylamide copolymers. IX. Preparation and characterization of the cationic derivatives of poly(acrylamide-co-N,N-dimethylacrylamide), poly(acrylamide-co-methacrylamide), and poly(acrylamide-co-N-t-butylacrylamide), J. Polym. Sci. A: Polym. Chem. 39 (2001) 2525–2535.
[4] G.J. Howard, F.L. Hudson, J. West, Water-soluble polymers as retention aids in a model papermaking system. I. Polyacrylamides, J. Appl. Polym. Sci. 21 (1977) 1–16.
[5] R.H. Pelton, L.H. Allen, The effects of some electrolytes on flocculation with a cationic polyacrylamide, Colloid Polym. Sci. 261 (1983) 485–492.
[6] G. Moody, The use of polyacrylamides in mineral processing, Miner. Eng. 5 (1992) 479–492.
[7] M. Smollen, Dewaterability of municipal sludge 1:a comparative study of specific resistance to filtration and capillary suction time as dewaterability parameters, Water SA 12 (1986) 127–132.
[8] H.F. Mark, N.M. Bikales, C.G. Overberger, G. Menges, Encyclopedia of polymer science and engineering, second ed., Willey, New York, 1985.
[9] R. Nicke, S. Pensold, H.-J. Hartman, M. Tappe, Polysiallyldimethylammonium chloride as a flocculating agent, Wochenbl. Paperfabr. 120 (1992) 559–564.
[10] W. Sun, G. Zhang, L. Pan, H. Li, A. Shi, Synthesis, characterization, flocculation properties of branched cationic polyacrylamide, Int'l J. Polym. Sci. 2013 (2013), Article ID 397027.
[11] F. Mabire, R. Audebert, C. Quivoron, Synthesis and solution properties of water soluble copolymers based on acrylamide and quaternary ammonium acrylic comonomer, Polymer 25 (1984) 1317–1322.
[12] D. Chen, Z. Liu, Y. Yue, W. Zhang, P. Wang, Dispersion copolymerization of acrylamide with quaternary ammonium cationic monomer in aqueous salt solution, Eur. Polym. J. 42 (2006) 1284–1297.

[13] M.S. Cho, B.K. Song, K.J. Yoon, Flocculation characteristics of copolymer of acrylamide with quaternary ammonium cationic monomer (running) flocculation by cationic polyacrylamide, J. Ind. Eng. Chem. 8 (2002) 131–137.
[14] B.K. Song, M.S. Cho, K.J. Yoon, D.C. Lee, Dispersion polymerization of acrylamide with quaternary ammonium cationic comonomer in aqueous solution, J. App. Polym. Sci. 87 (2003) 1101–1108.
[15] I.J. Hobson, W.J. Feast, Polyamidoamine hyperbranched systems: synthesis, structure and characterization, Polymer 40 (1999) 1279–1297.
[16] J.-H. Shin, S.H. Han, C. Sohn, S.K. Ow, S. Mah, Highly branched cationic polyelectrolytes filler flocculation, Tappi. J. 80 (1997) 179–185.
[17] K.A. Klimchuk, M.B. Hocking, S. Lowen, Water-soluble acrylamide copolymers. VII. Preparation and characterization of poly(methacrylamide-co-acrylamide), J. Polym. Sci. A: Polym. Chem. 38 (2000) 3128–3145.
[18] J.C. Giddings, Field-flow fractionation: analysis of macromolecular, colloidal, and particulate materials, Science 260 (1993) 1456–1465.
[19] K.-G. Wahlund, J.C. Giddings, Properties of an asymmetrical flow field-flow fractionation channel having one permeable wall, Anal. Chem. 59 (1987) 1332–1339.
[20] S.K. Ratanathanawongs, J.C. Giddings, Dual-field and flow-programmed lift hyperlayer field-flow fractionation, Anal. Chem. 64 (1992) 6–15.
[21] D. Kang, S. Oh, S.-M. Ahn, B.-H. Lee, M.H. Moon, Proteomic analysis of exosomes from human neural stem cells by flow field-flow fractionation and nanoflow liquid chromatography-tandem mass spectrometry, J. Proteome Res. 7 (2008) 3475–3480.
[22] J.S. Yang, J.Y. Lee, M.H. Moon, High speed size sorting of subcellular organelles by flow field-flow fractioantion, Anal. Chem. 87 (2015) 6342–6348.
[23] J.C. Giddings, Field flow fractionation. A versatile method for the characterization of macromolecular and particulate materials, Anal. Chem. 53 (1981) 1170A–1178A.
[24] B. Wittgren, K.-G. Wahlund, Fast molecular mass and size characterization of polysaccharides using asymmetrical flow field-flow fractionation-multiangle light scattering, J. Chromatogr. A 760 (1997) 205–218.
[25] B. Hecker, P.D. Fawell, A. Jefferson, J.B. Farrow, Flow field-flow fractionation of high-molecular-mass polyacrylamide, J. Chromatogr. A 837 (1999) 139–151.
[26] M. van Bruijinsvoort, K.-G. Wahlund, G. Nilsson, W.Th. Kok, Retention behaviour of amylopectins in asymmetrical flow field-flow fractionation studied by multi-angle light scattering detection, J. Chromatogr. A 925 (2001) 171–182.
[27] S. Lee, P.-O. Nilsson, G.S. Nilsson, K.-G. Wahlund, Development of asymmetrical flow field-flow fractionation–multi angle laser light scattering analysis for molecular mass characterization of cationic potato amylopectin, J. Chromatogr. A 1011 (2003) 111–123.
[28] H. Lee, I.-H. Cho, M.H. Moon, Effect of dissolution temperature on the structures of sodium hyaluronate by flow field-flow fractionation/multiangle light scattering, J. Chromatogr. A 1131 (2006) 185–191.
[29] D.Y. Shin, E. Hwang, I.-H. Cho, M.H. Moon, Molecular weight and structure characterization of sodium hyaluronate and its gamma radiation degradation products by flow field-flow fractionation and on-line multiangle light scattering, J. Chromatogr. A 1160 (2007) 270–275.
[30] M.H. Moon, Flow field-flow fractionation and multiangle light scattering for ultrahigh molecular weight sodium hyaluronate characterization, J. Sep. Sci. 33 (2010) 3519–3529.
[31] M. Ali, E. Hwang, I.-H. Cho, M.H. Moon, Characterization of sodium hyaluronate blends using frit inlet asymmetrical flow field-flow fractionation & multiangle light scattering, Anal. Bioanal. Chem. 402 (2012) 1269–1276.
[32] B. Kim, S. Woo, Y.-S. Park, E. Hwang, M.H. Moon, Ionic strength effect on molecular structure of hyaluronic acid investigated by flow field-flow fractionation and multiangle light scattering, Anal. Bioanal. Chem. 407 (2015) 1327–1334.
[33] M.H. Moon, H. Kwon, I. Park, Stopless flow injection in asymmetrical flow field-flow fractionation using a frit inlet, Anal. Chem. 69 (1997) 1436–1440.
[34] P. Reschiglian, A. Zattoni, B. Roda, S. Casolari, M.H. Moon, J. Lee, J. Jung, K. Rodmalm, G. Cenacchi, Bacteria Sorting by Field-Flow Fractionation: Application to Whole-Cell *E. coli Vaccine Strains*, Anal. Chem. 74 (2002) 4895–4904.
[35] H. Dou, Y.-J. Lee, E.C. Jung, B.-C. Lee, S. Lee, Study on steric transition in asymmetrical flow field-flow fractionation and application to characterization of high-energy material, J. Chromatogr. A 1304 (2013) 211–219.